ACS MATERIALS LETTERS

www.acsmaterialsletters.org

LETTER

$Rb_3B_{11}P_2O_{23}$: Materials Design of a New Chemically Benign Deep-Ultraviolet Nonlinear Optical Material

Haonan Liu, Hongping Wu, Zhanggui Hu, Jiyang Wang, Yicheng Wu, P. Shiv Halasyamani,* and Hongwei Yu*

Cite This: *ACS Materials Lett.* 2023, 5, 155−161

Read Online

ACCESS | Metrics & More | Article Recommendations | Supporting Information

ABSTRACT: **Deep-ultraviolet (DUV) coherent light is urgently needed for many important technological applications such as lithography and advanced scientific instruments. Its generation, however, strongly depends on the frequency conversion of nonlinear optical (NLO) materials. Currently, $KBe_2BO_3F_2$ (KBBF) is sole material that can produce the DUV coherent light by direct second-harmonic generation (SHG), i.e., sixth harmonic generation of Nd:YAG (1064 nm/6 = 173 nm). The strong layering growth habit, and the highly toxicity of BeO make the safe growth of KBBF a great challenge. In this communication, we report the first chemically benign DUV three-dimensional mixed-coordinated borophosphate $Rb_3B_{11}P_2O_{23}$ (RBPO). This material inherits all the excellent structural genes of KBBF and achieves comparable optical properties, such as a large SHG response (2.5 × KDP; 1.2 × KDP for KBBF), short absorption edge (168 nm; 147 nm for KBBF) and suitable birefringence (0.071@1064 nm; 0.077@1064 nm for KBBF). More importantly, RBPO melts congruently and can overcome all the processing limitations of KBBF. Theoretical calculations and structure analysis reveal that its superior optical properties can be attributed to the KBBF-like $[B_4P_2O_{11}]_\infty$ layers, where NLO-active B_3O_7 groups adopt a coplanar configuration with well-ordered arrangement. These indicate RBPO will be the new generation of DUV NLO crystal.**

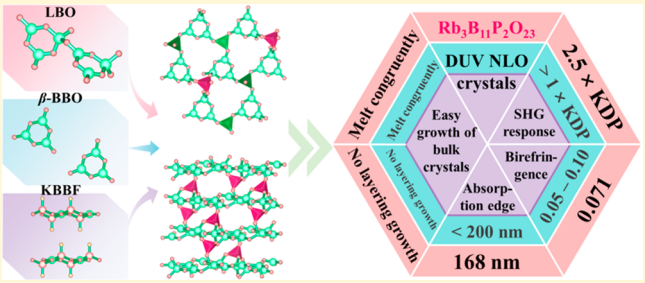

Deep-ultraviolet (DUV) coherent lights, λ < 200 nm, play an indispensable role in the development of laser micromachining, semiconductor manufacturing, and scanning tunneling microscopy.[1−8] For solid-state lasers, the most effective way to obtain DUV coherent light, i.e., the sixth harmonic of Nd:YAG (1064 nm), 177.3 nm, is through the cascaded frequency conversion of a nonlinear optical (NLO) material. However, in order to realize the effective frequency conversion, the DUV NLO material must satisfy the following critical requirements: (i) short absorption edge (λ_{cutoff} < 200 nm), (ii) sufficient birefringence (Δn = 0.05−0.10) for index phase-matching, (iii) large second-harmonic generation (SHG) coefficient (d_{ij} > d_{36} (KH_2PO_4 (KDP)) = 0.39 pm/V), (iv) chemical stability with a large laser damage threshold, and (v) easy growth of bulk high-quality single crystals. Combining the above in a single DUV NLO material is an ongoing challenge.[9−20]

Borates are a preferred NLO materials class owing to the presence of good "optical groups", e.g., π-conjugated BO_3, B_3O_6, and B_3O_7 moieties.[21−26] Over the past decades, a series of notable UV borate NLO materials have been synthesized, including β-BaB_2O_4 (β-BBO),[27] LiB_3O_5 (LBO),[28] and $CsLiB_6O_{10}$ (CLBO).[29] Crystals of these materials, however, cannot be used to generate DUV coherent radiation owing to the absorption edge for β-BBO (189 nm), and the small birefringences for LBO and CLBO, i.e., 0.0399 and 0.0498@1064 nm, respectively.[29] These issues are caused by the local B−O bonding, as well as borate connectivity. To date, $KBe_2BO_3F_2$ (KBBF)[30] is still the sole material that can achieve the output of DUV coherent light by SHG. The excellent optical properties of KBBF can be attributed to the unique $[Be_2BO_3F_2]_\infty$ layers, where all the BO_3 groups are aligned in the same orientation that results in the observed SHG response (1.2 × KDP) and birefringence (0.077@1064 nm). The

Received: October 1, 2022
Accepted: December 8, 2022
Published: December 12, 2022

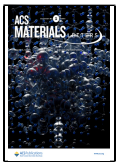

https://doi.org/10.1021/acsmaterialslett.2c00929
ACS Materials Lett. 2023, 5, 155−161

dangling B−O bonds are eliminated through the alternative connection of BeO_3F tetrahedra and BO_3 groups that results in very short absorption edge of 147 nm. Unfortunately, KBBF has a very strong layered habit that makes crystal growth very difficult. In fact, the maximum crystal thickness that has been grown is less than 4 mm. In addition, the Be-compounds are also classified as a type-I carcinogen according to the International Agency for Research on Cancer.[31] All of these attributes seriously hinder the commercial use of KBBF.

A class of materials that may provide opportunities for DUV NLO materials are borophosphates. Borophosphates integrate the advantages of borates and phosphates, e.g., the absorption edge of the NLO material BPO_4 is 130 nm with an SHG response of 2.0 × KDP. However, BPO_4 exhibits a very small birefringence, 0.005@1064 nm, arising from the tetrahedral coordination of boron and phosphorus, i.e., BO_4 and PO_4 groups. As such, BPO_4 cannot be phase-matched in the DUV.[32,33] In previous research, we developed the zincoborate-phosphate, $Ba_3(ZnB_5O_{10})PO_4$.[34,35] It can exhibit larger SHG response (~4 × KDP). But its birefrigence, 0.034@532 nm, is still too small for the DUV phase-matching. Recently, we have suggested that through increasing the B/P ratio to design mixed-coordinated borophosphates one can enhance the anisotropic polarization of structures and increase the birefringence. We have successfully synthesized a series of borophosphates with larger birefringences, such as $K_3B_4PO_{10}$ (0.0445@532 nm)[36] and $NH_4(B_6PO_{10}(OH)_4)\cdot H_2O$ (0.0951@532 nm).[37] But owing to the antiparallel arrangement of their basic building units (BBUs), most of these borophosphates crystallize in centrosymmetric (CS) space groups or exhibit relatively weak SHG responses.[38]

In this work, we have successfully synthesized the first three-dimensional (3D) noncentrosymmetric (NCS) DUV mixed-coordinated borophosphate, $Rb_3B_{11}P_2O_{23}$ (RBPO). Our design strategy was based on the structural integration of three classic NLO crystals, β-BBO, LBO, and KBBF. We (i) replaced the B_3O_6 units in β-BBO by the B_3O_7 units in LBO to maintain the coplanar arrangement of NLO-active BBUs to obtain moderate birefringence and strong SHG response; (ii) utilized the BO_4 and PO_4 tetrahedra to eliminate the dangling bonds of the B_3O_7 units to construct the $[Be_2BO_3F_2]_\infty$-like layer to blueshift the absorption edge; and (iii) bridged the adjacent layers by B−O−P bonds forming the 3D framework to remove the layer habit of KBBF. As expected, RBPO exhibits comparable, or even superior, NLO properties compared with the sole DUV NLO material KBBF. These excellent NLO properties include a suitable birefringence, 0.071@1064 nm, a short absorption edge (168 nm), and a large SHG response (2.5 × KDP). Importantly, a 3D structural framework and congruently melting thermal property are also observed. These demonstrate RBPO is a new promising DUV NLO material. In this report, we present the synthesis, crystal structure, thermal behavior, linear and NLO properties, as well as structure−property relationships in RBPO.

RBPO was synthesized by conventional solid-state methods, and the purity of the sample was verified by powder X-ray diffraction (PXRD) (Figure S1). Furthermore, the pure polycrystalline samples were analyzed by thermogravimetric and differential scanning calorimetry (TG/DSC) (Figure S2a). Clearly, RBPO contains only one endothermic peak at 665 °C on its DSC curve, and no weight loss is observed on the TG curve. These suggest RBPO melts congruently. In order to verify its congruently melting property, RBPO was melted at 680 °C and then cooled to room temperature. The PXRD patterns before and after melting are identical (Figure S2b), further demonstrating that RBPO melt congruently. Owing to the congruent-melting behavior, its single crystals can be grown from the stoichiometric melt. Figure S3 show the photograph of RBPO crystal. Clearly, RBPO has no layer habit with a large thickness-length ratio of ~0.75. The best thickness-length ratio of in reported KBBF crystals is only ~0.076. These exhibit RBPO can indeed overcome the layer habit and the highly toxic issues of KBBF.

The structure of RBPO was determined by single-crystal XRD, with the structural data is given in Table S1. The asymmetric unit of RBPO contains three Rb, eleven B, two P, and twenty-three O atoms (Table S2). The crystal structure is shown in Figure 1. The BBU of RBPO is a $[B_4P_2O_{16}]$ group

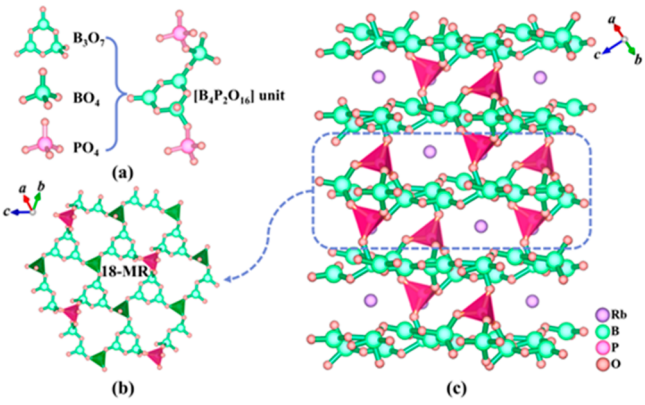

Figure 1. Crystal structure of RBPO. (a) B_3O_7, BO_4, PO_4, and $[B_4P_2O_{16}]$ units. (b) 2D $[B_4P_2O_{11}]_\infty$ layer with 18-MRs. (c) 3D $[B_{11}P_2O_{23}]_\infty$ framework with Rb^+ cations filled in the void space.

(Figure 1a), constructed by one B_3O_7, one BO_4 and two PO_4 unit(s). The B−O and P−O bond lengths range from 1.326(13) to 1.584(12) Å and from 1.507(7) to 1.539(7) Å, respectively. Three $[B_4P_2O_{16}]$ units are connected through corner-sharing oxygen to form a large 18-membered ring (MR). These rings are additionally connected by sharing O atoms to create a $[B_4P_2O_{11}]_\infty$ layer (Figure 1b). Finally, the $[B_4P_2O_{11}]_\infty$ layers are bridged by B−O−P bonds to form the 3D $[B_{11}P_2O_{23}]_\infty$ framework (Figure 1c). The Rb^+ cations fill the void space of the $[B_{11}P_2O_{23}]_\infty$ framework to balance the residual charges. The Rb−O bond distances range from 2.852(7) to 3.503(9) Å (Table S3). The reasonability of the structure is verified by the Raman spectrum (Figure S4).[39−42] Bond valence calculations[43] (Rb, 0.87−0.99; B, 3.03−3.14; P, 4.91−4.93; and O, 1.83−2.13) confirm that the Rb, B, P, and O atoms are in oxidation states of +1, +3, +5, and −2, respectively.

In order to obtain the DUV and IR absorption edges, the optical transmission spectrum of RBPO single-crystal sample was recorded with a polish 1 mm thick $(\bar{1}11)$ plate. As seen in Figure 2a, it possesses wide transparency range, 168−3500 nm. This indicates RBPO is DUV transparent, and its UV absorption edge is comparable with other DUV NLO materials, such as KBBF (147 nm),[30] LBO (160 nm),[28] $Rb_3B_8PO_{16}$ (175 nm),[38] and β- BBO (189 nm).[27] In addition, the birefringence of RBPO was measured by using a cross-polarizing microscope. The following formula $R = \Delta n \times d$, where R, Δn and d are the retardation, birefringence, and thickness of the crystal, respectively, was used to determine the

https://doi.org/10.1021/acsmaterialslett.2c00929
ACS Materials Lett. 2023, 5, 155−161

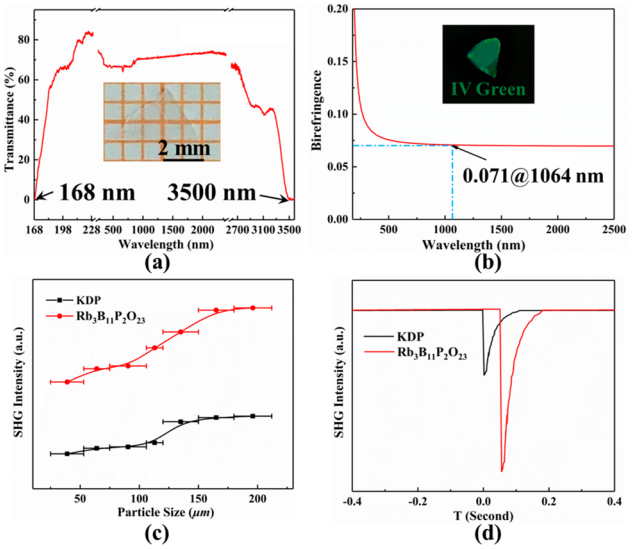

Figure 2. (a) Transmission spectra on single crystals of RBPO (Inset: Photographs of RBPO spectroscopy crystals). (b) The calculated birefringence (Δ*n*) curves and measured by cross-polarized light for RBPO crystal (inset). (c, d) Powder SHG measurements at 1064 nm.

birefringence.[44] In the measurement, the crystal of RBPO with a thickness of 24.6 mm was used (Figure S5a). The orientation of such autilized crystal was determined as $(\bar{1}11)$ by using the "Index Crystal Faces" program in Bruker SMARTAPEX III (Figure S5b). And the fourth-order green interference color was observed by the cross-polarized light microscope (Figure 2b). By comparing with the Michal–Levy chart, *R* is approximately 1800 nm. Consequently, the birefringence of RBPO is about 0.073 in the visible region. Remarkably, this value represents the in-plane birefringence of the measured crystal, and not the largest birefringence. We calculated the birefringence of RBPO resulting in values ranging from 0.071@1064 nm to 0.075@532 nm. These birefringence values are suitable for DUV phase matching. Additionally, the birefringence of RBPO is larger than LBO (0.0399@1064 nm),[28] CLBO (0.0498@1064 nm),[29] and CsB_3O_5 (0.0587@1064 nm),[45] and is even comparable to the unique practical DUV NLO material, KBBF (0.077@1064 nm).[30] The large birefringence value for RBPO indicates a wide phase-matching wavelength range. As shown in Figure S6a, the shortest phase-matching wavelength of RBPO is down to about 205 nm, which presents the shortest value in the reported borophosphates (Figure S6b).

In order to achieve the effective frequency conversion in DUV region, a large phase-mathcing SHG response (>1 × KDP) is also nessessary. The powder SHG measurements of RBPO was carried out by the Kurtz–Perry method.[46] As shown in Figure 2c and d, RBPO is type-I phase-matchable, and its SHG response is 2.5 × KDP at 1064 nm. These indicate it can exhibit large enough SHG response as a DUV NLO crystal, and its SHG response is even larger than double that of KBBF (Table 1). In order to understand the origin of the large SHG response of RBPO, the first-principles calculations are also carried out.[47,48] Clearly, RBPO has an indirect band gap of 5.72 eV (Figure S7a), smaller than the experimental result, which can be attributed to the underestimation of E_g by DFT calculations. As shown in Figure S7b, the upper parts of valence band (VB) from −10 to 0 eV for RBPO is mainly composed of the O 2p orbitals, mixing with small amounts of B 2p and P 3p, whereas the bottom of the conductive band (CB) mostly originates from B 2p and O 2p states. Since the electronic states near in the energy band gap determine the optical properties in UV and DUV regions, the B–O units determine the SHG effect of RBPO. Meanwhile, the electron localization function (ELF)[49] used to visualize interatomic interactions was also computed in RBPO, *β*-BBO, LBO, and KBBF. As shown in Figure S7c–f, four compounds exhibit clover-shaped electron densities about the oxide anions comprising the BO_3 units, which indicate the discernible asymmetric localization of charge density about the O sites in BO_3 units activated by acentric atomic distortions contributes to their high SHG intensity.

It is clear that RBPO meets all the rigorous criteria for a technologically applicable DUV NLO crystal, including large SHG response (2.5 × KDP), suitable birefringence (0.071@1064 nm), short absorption edge (168 nm), 3D framework structure, and congruently melting behavior (Figure 3). All of

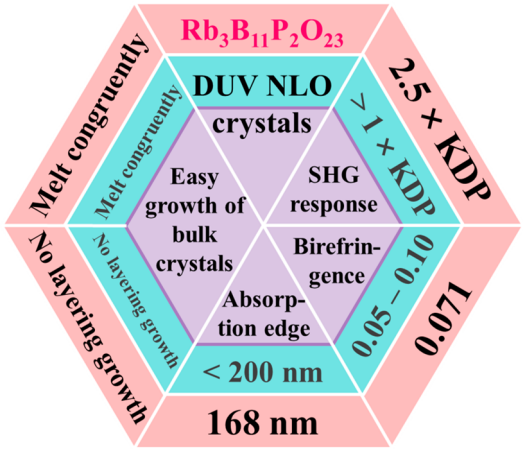

Figure 3. Excellent overall performances of RBPO.

Table 1. Comparison of the Dimensionality, SHG Responses, Birefringences, Absorption Edges, and Thermal Behavior among RBPO and Other Practical and Emerging DUV NLO Materials

dimensionality	compounds	SHG response (×KDP)	birefringence (@1064 nm)	absorption edge (nm)	melting behavior
single layer	$KBe_2BO_3F_2$[30]	1.2	0.077	147	incongruent
	CsB_4O_6F[19]	1.9	0.113	155	congruent
	$NH_4B_4O_6F$[17]	3	0.117	156	incongruent
	$(NH_4)_2B_4SO_{10}$[51]	1.1	0.053	184	incongruent
double layer	$Sr_2Be_2B_2O_7$[1]	4.15	0.060	165	incongruent
	$Rb_3B_8PO_{16}$[38]	0.5	0.071	175	congruent
3D framework	**$Rb_3B_{11}P_2O_{23}$[this work]**	**2.5**	**0.071**	**168**	**congruent**

https://doi.org/10.1021/acsmaterialslett.2c00929
ACS Materials Lett. 2023, 5, 155–161

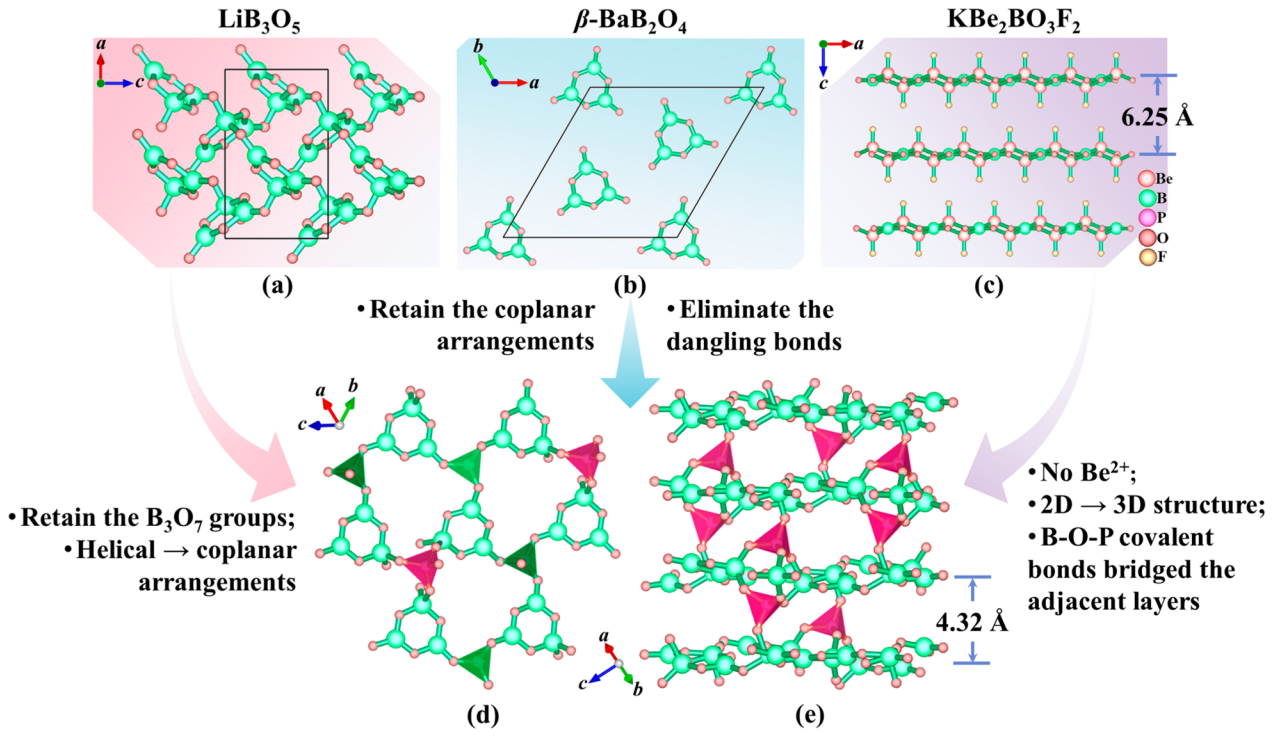

Figure 4. Crystallographic structure comparisons: (a) LBO, (b) β-BBO, (c) KBBF, (d) $[B_4P_2O_{11}]_\infty$ layer, and (e) RBPO.

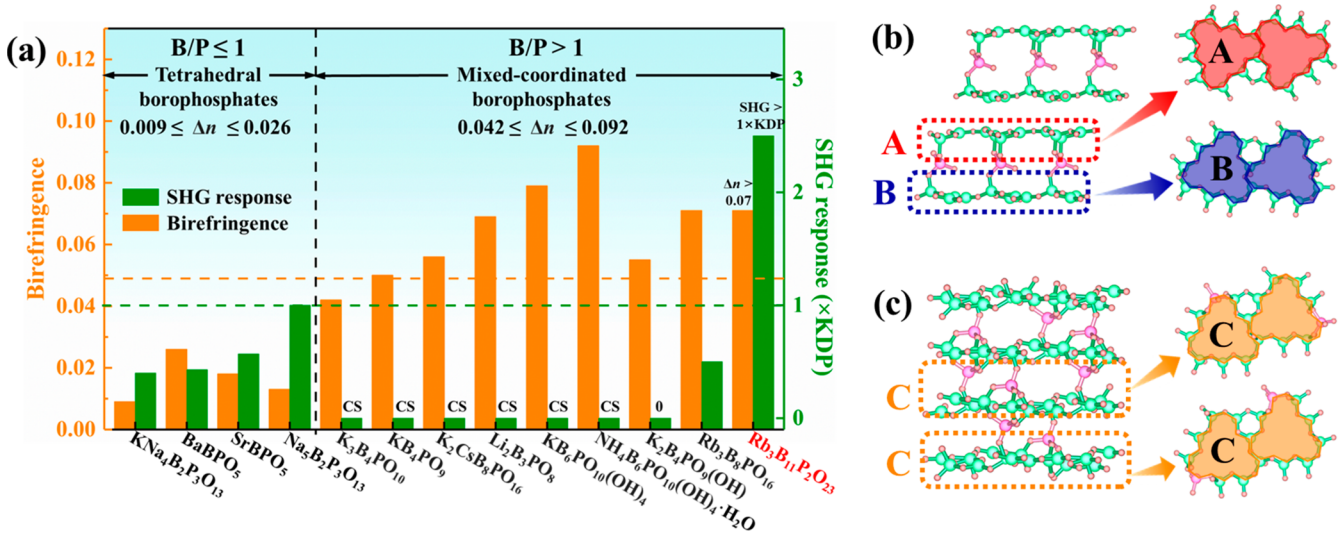

Figure 5. (a) Comparison of reported DUV transparent borophosphates birefringence values and SHG responses, respectively. (b) 2D double-layered structure of $Rb_3B_8PO_{16}$ constructed by the antiparallel arrangement of layers "A" and "B". (c) 3D framework structure of RBPO built by the parallel arranged layers "C".

these good features will favor for the application of RBPO as a promising DUV NLO crystal. The excellent properties of RBPO can also be attributed to its unique crystal structure that integrates all the favorable structural features of the classic UV NLO crystals, LBO, β-BBO, and KBBF. First, RBPO has similar BBUs to LBO, i.e., π-conjugated B_3O_7 units. Remarkably, the B_3O_7 units in RBPO do not adapt in a helical arrangement as observed in LBO, (Figure 4a), but are arranged in a coplanar manner (Figure 4d). This arrangement results in a large SHG response and birefringence, similar to what is observed in β-BBO (Figure 4b). In addition, the terminal O atoms of B_3O_7 units in RBPO are fully bonded by the B−O−P covalent bonds to form the $[B_4P_2O_{11}]_\infty$ planar layer (Figure 4d), and the adjacent $[B_4P_2O_{11}]_\infty$ planar layers are bridged by the B−O−P covalent bonds forming the 3D framework (Figure 4e). This full connectivity removes any dangling oxygen bonds and blue-shifts the absorption edge, and also overcomes the layer-habit issues in KBBF. More importantly, from KBBF to RBPO, the K−F ionic bonds are substituted by the B−O−P covalent bonds that reinforce the interlayer interactions, and reduce the distances between the adjacent layers from 6.25 Å in KBBF (Figure 4c) to 4.32 Å in RBPO (Figure 4e). The B−O−P covalent bonds increase the number density of NLO-active BO_3 units in a unit cell, RBPO: 0.0123, KBBF: 0.0094, resulting in the enhancement of the SHG response.

https://doi.org/10.1021/acsmaterialslett.2c00929
ACS Materials Lett. 2023, 5, 155−161

Furthermore, in the structure of RBPO, it contains BO_4 and PO_4 tetrahedra as well as π-conjugated B_3O_7 units, so it represents the new type of mixed-coordinated NLO borophosphates. As shown in Figure 5a, compared with tetrahedral borophosphates that only contain the tetrahedral-coordinated BO_4 and PO_4 tetrahedra as BBUs, the mixed-coordinated borophosphates are generally able to exhibit larger birefringence because their structures can contain the π-conjugated planar groups. Accordingly, most of mixed-coordinated borophosphates exhibit larger birefringence, as observed in $K_3B_4PO_{10}$,[36] $Li_2B_3PO_8$,[50] $KB_6PO_{10}(OH)_4$,[38] $NH_4B_6PO_{10}(OH)_4{\cdot}H_2O$,[37] their birefringences generally range from 0.042 to 0.092@1064 nm, whereas the birefringences of tetrahedral borophosphates are usually smaller than 0.03@1064 nm (Table S4, Figure 5a). Therefore, it is easier for mixed-coordinated borophosphates to achieve the DUV phase-matching. Remarkably, most of the previously reported mixed-coordinated borophosphates crystallize in CS space groups or exhibit weak SHG responses (Table S5) owing to the antiparallel arrangement of their BBUs, as observed in recently reported $Rb_3B_8PO_{16}$ (Figure 5b). However, different form the previously reported mixed-coordinated borophosphates, RBPO integrates the structural merits of three classic NLO crystals, i.e., the BBUs, $[B_4P_2O_{11}]_\infty$ layers in RBPO has the aligned arrangements (Figure 5c), which makes it display the largest SHG response (2.5 × KDP) in the reported borophosphates (Table S4, Figure 5a). More importantly, this good feature also favors it break through all the limitation of borophosphates as DUV NLO crystals, which indicates mixed-coordinated borophosphates will be a new direction for exploring the promising DUV NLO crystals. In addition, comparing the structures and functional properties of RBPO with other DUV NLO crystals, we also conclude that RBPO are quite rare materials that can meet all rigorous requirements for DUV NLO applications (Table 1).

To summarize, a new chemically benign DUV mixed-coordinated borophosphate, RBPO has been successfully designed and synthesized. Structurally, RBPO contains the BO_4 and PO_4 tetrahedra, as well as the π-conjugated B_3O_7 units, so it belongs to the mixed-coordinated borophosphates. Compared to the classic NLO crystals, RBPO also exhibits all the positive optical attributes of β-BBO, LBO and KBBF, which make RBPO exhibit comparable NLO properties with the currently sole practical DUV NLO crystal KBBF, including a strong SHG response (2.5 × KDP), a short UV absorption edge (168 nm), and a moderate birefringence (0.071@1064 nm). More importantly, RBPO melts congruently, and the introduction of B−O−P covalent bonds between the adjacent layers can enhance interlayer interaction force, enabling the facile growth of large single crystals with better growth habit. Therefore, we believe that RBPO will be a promising DUV NLO crystal, and the mixed-coordinated borophosphates will represent the new direction for the design of next generation DUV NLO crystals.

■ ASSOCIATED CONTENT

Supporting Information

The Supporting Information is available free of charge at https://pubs.acs.org/doi/10.1021/acsmaterialslett.2c00929.

Crystal data and structure refinement, atomic coordinates, equivalent isotropic displacement parameters, bond valence sum, table of bond lengths and angles for RBPO, a summary of reported DUV transparent borophosphates, PXRD patterns, photograph, DSC/TG curves, IR, Raman, thickness of single crystal, band structure, DOS and PDOS, and ELF maps for RBPO. (PDF)

Crystallographic information file for RBPO (CIF)

■ AUTHOR INFORMATION

Corresponding Authors

P. Shiv Halasyamani − *Department of Chemistry, University of Houston, Houston, Texas 77204-5003, United States;* orcid.org/0000-0003-1787-1040; Email: psh@uh.edu

Hongwei Yu − *Tianjin Key Laboratory of Functional Crystal Materials, Institute of Functional Crystal, Tianjin University of Technology, Tianjin 300384, China;* orcid.org/0000-0002-5607-0628; Email: hwyu15@gmail.com

Authors

Haonan Liu − *Tianjin Key Laboratory of Functional Crystal Materials, Institute of Functional Crystal, Tianjin University of Technology, Tianjin 300384, China*

Hongping Wu − *Tianjin Key Laboratory of Functional Crystal Materials, Institute of Functional Crystal, Tianjin University of Technology, Tianjin 300384, China;* orcid.org/0000-0003-0975-1700

Zhanggui Hu − *Tianjin Key Laboratory of Functional Crystal Materials, Institute of Functional Crystal, Tianjin University of Technology, Tianjin 300384, China*

Jiyang Wang − *Tianjin Key Laboratory of Functional Crystal Materials, Institute of Functional Crystal, Tianjin University of Technology, Tianjin 300384, China*

Yicheng Wu − *Tianjin Key Laboratory of Functional Crystal Materials, Institute of Functional Crystal, Tianjin University of Technology, Tianjin 300384, China*

Complete contact information is available at: https://pubs.acs.org/10.1021/acsmaterialslett.2c00929

Author Contributions

The manuscript was written through contributions of all authors.

Notes

The authors declare no competing financial interest.

■ ACKNOWLEDGMENTS

This work is supported by the National Natural Science Foundation of China (Grant No. 22071179, 92163207, 52172006, 51972230, 51890864, 61835014, 51890865) and Natural Science Foundation of Tianjin (Grant No. 21JCJQJC00090 and 20JCJQJC00060). P.S.H. thanks the Welch Foundation Grant (E-1457) and the NSF (DMR-2002319) for support.

■ REFERENCES

(1) Chen, C.; Wang, Y.; Wu, B.; Wu, K.; Zeng, W.; Yu, L. Design and Synthesis of an Ultraviolet-Transparent Nonlinear Optical Crystal $Sr_2Be_2B_2O_7$. *Nature* **1995**, *373*, 322−324.

(2) Tran, T. T.; Young, J.; Rondinelli, J. M.; Halasyamani, P. S. Mixed-Metal Carbonate Fluorides as Deep-Ultraviolet Nonlinear Optical Materials. *J. Am. Chem. Soc.* **2017**, *139*, 1285−1295.

(3) Huang, C.; Mutailipu, M.; Zhang, F.; Griffith, K. J.; Hu, C.; Yang, Z.; Griffin, J. M.; Poeppelmeier, K. R.; Pan, S. Expanding the Chemistry of Borates with Functional $[BO_2]^-$ Anions. *Nat. Commun.* **2021**, *12*, 2597.

(4) Wu, C.; Yang, G.; Humphrey, M. G.; Zhang, C. Recent Advances in Ultraviolet and Deep-Ultraviolet Second-Order Nonlinear Optical Crystals. *Coord. Chem. Rev.* **2018**, *375*, 459−488.
(5) Zhao, S.; Gong, P.; Bai, L.; Xu, X.; Zhang, S.; Sun, Z.; Lin, Z.; Hong, M.; Chen, C.; Luo, J. Beryllium-Free $Li_4Sr(BO_3)_2$ for Deep-Ultraviolet Nonlinear Optical Applications. *Nat. Commun.* **2014**, *5*, 4019.
(6) Halasyamani, P. S.; Rondinelli, J. M. The Must-Have and Nice-to-Have Experimental and Computational Requirements for Functional Frequency Doubling Deep-UV Crystals. *Nat. Commun.* **2018**, *9*, 2972.
(7) Zhang, X.; Cao, D.; Yang, D.; Wang, Y.; Wu, K.; Lee, M. H.; Zhang, B. Finding the First Squarates Nonlinear Optical Crystal $NaHC_4O_4{\cdot}H_2O$ with Strong Second Harmonic Generation and Giant Birefringence. *ACS Mater. Lett.* **2022**, *4*, 572−576.
(8) Kang, L.; Lin, Z. Deep-Ultraviolet Nonlinear Optical Crystals: Concept Development and Materials Discovery. *Light Sci. Appl.* **2022**, *11*, 201.
(9) Xiong, L.; Wu, L. M.; Chen, L. A General Principle for DUV NLO Materials: π-Conjugated Confinement Enlarges Band Gap. *Angew. Chem., Int. Ed.* **2021**, *60*, 25063−25067.
(10) Sha, H.; Su, R.; Xiong, Z.; Wang, Z.; Shan, P.; He, C.; Yang, X.; Long, X. Borosilicate Crystal $LaBSiO_5$: A New Promising Ultraviolet Quasiphase Matching Material. *Adv. Opt. Mater.* **2021**, *9*, 2100080.
(11) Wang, Y.; Zhang, B.; Yang, Z.; Pan, S. Cation-Tuned Synthesis of Fluorooxoborates: Towards Optimal Deep-Ultraviolet Nonlinear Optical Materials. *Angew. Chem., Int. Ed.* **2018**, *57*, 2150−2154.
(12) Zhang, Z.; Wang, Y.; Zhang, B.; Yang, Z.; Pan, S. Polar Fluorooxoborate, NaB_4O_6F: A Promising Material for Ionic Conduction and Nonlinear Optics. *Angew. Chem., Int. Ed.* **2018**, *57*, 6577−6581.
(13) Wu, H.; Yu, H.; Yang, Z.; Hou, X.; Su, X.; Pan, S.; Poeppelmeier, K. R.; Rondinelli, J. M. Designing a Deep-Ultraviolet Nonlinear Optical Material with a Large Second Harmonic Generation Response. *J. Am. Chem. Soc.* **2013**, *135*, 4215−4218.
(14) Wu, H.; Pan, S.; Poeppelmeier, K. R.; Li, H.; Jia, D.; Chen, Z.; Fan, X.; Yang, Y.; Rondinelli, J. M.; Luo, H. $K_3B_6O_{10}Cl$: A New Structure Analogous to Perovskite with a Large Second Harmonic Generation Response and Deep UV Absorption Edge. *J. Am. Chem. Soc.* **2011**, *133*, 7786−7790.
(15) Zou, G.; Ok, K. M. Novel Ultraviolet (UV) Nonlinear Optical (NLO) Materials Discovered by Chemical Substitution-Oriented Design. *Chem. Sci.* **2020**, *11*, 5404−5409.
(16) Huang, H.; Yao, J.; Lin, Z.; Wang, X.; He, R.; Yao, W.; Zhai, N.; Chen, C. $NaSr_3Be_3B_3O_9F_4$: A Promising Deep-Ultraviolet Nonlinear Optical Material Resulting from the Cooperative Alignment of the $[Be_3B_3O_{12}F]^{10-}$ Anionic Group. *Angew. Chem., Int. Ed.* **2011**, *50*, 9141−9144.
(17) Shi, G.; Wang, Y.; Zhang, F.; Zhang, B.; Yang, Z.; Hou, X.; Pan, S.; Poeppelmeier, K. R. Finding the Next Deep-Ultraviolet Nonlinear Optical Material: $NH_4B_4O_6F$. *J. Am. Chem. Soc.* **2017**, *139*, 10645−10648.
(18) Zhang, B.; Shi, G.; Yang, Z.; Zhang, F.; Pan, S. Fluorooxoborates: Beryllium-Free Deep-Ultraviolet Nonlinear Optical Materials without Layered Growth. *Angew. Chem., Int. Ed.* **2017**, *56*, 3916−3919.
(19) Wang, X.; Wang, Y.; Zhang, B.; Zhang, F.; Yang, Z.; Pan, S. CsB_4O_6F: A Congruent-Melting Deep-Ultraviolet Nonlinear Optical Material by Combining Superior Functional Units. *Angew. Chem., Int. Ed.* **2017**, *56*, 14119−14123.
(20) Mutailipu, M.; Zhang, M.; Zhang, B.; Wang, L.; Yang, Z.; Zhou, X.; Pan, S. $SrB_5O_7F_3$ Functionalized with $[B_5O_9F_3]^{6-}$ Chromophores: Accelerating the Rational Design of Deep-Ultraviolet Nonlinear Optical Materials. *Angew. Chem., Int. Ed.* **2018**, *57*, 6095−6099.
(21) Gao, M.; Wu, H.; Yu, H.; Hu, Z.; Wang, J.; Wu, Y. $BaYOBO_3$: A Deep-Ultraviolet Rare-Earth Oxy-Borate with a Large Second Harmonic Generation Response. *Sci. China Chem.* **2021**, *64*, 1184−1191.
(22) Yu, H.; Wu, H.; Pan, S.; Yang, Z.; Hou, X.; Su, X.; Jing, Q.; Poeppelmeier, K. R.; Rondinelli, J. M. $Cs_3Zn_6B_9O_{21}$: A Chemically Benign Member of the KBBF Family Exhibiting the Largest Second Harmonic Generation Response. *J. Am. Chem. Soc.* **2014**, *136*, 1264−1267.
(23) Jin, C.; Li, F.; Cheng, B.; Qiu, H.; Yang, Z.; Pan, S.; Mutailipu, M. Double-Modification Oriented Design of a Deep-UV Birefringent Crystal Functionalized by $[B_{12}O_{16}F_4(OH)_4]$ Clusters. *Angew. Chem., Int. Ed.* **2022**, *61*, e202203984.
(24) Wang, X.; Zhang, F.; Gao, L.; Yang, Z.; Pan, S. Nontoxic KBBF Family Member $Zn_2BO_3(OH)$: Balance between Beneficial Layered Structure and Layer Tendency. *Adv. Sci.* **2019**, *6*, 1901679.
(25) Li, S.; Liu, X.; Wu, H.; Song, Z.; Yu, H.; Lin, Z.; Hu, Z.; Wang, J.; Wu, Y. $Ba_4Ca(B_2O_5)_2F_2$: π-Conjugation of B_2O_5 in the Planar Pentagonal Layer Achieving Large Second Harmonic Generation of Pyro-Borate. *Chem. Sci.* **2021**, *12*, 13897−13901.
(26) Liu, R.; Wu, H.; Yu, H.; Hu, Z.; Wang, J.; Wu, Y. $K_5Mg_2La_3(BO_3)_6$: An Efficient, Deep-Ultraviolet Nonlinear Optical Material. *Chem. Mater.* **2021**, *33*, 4240−4246.
(27) Chen, C.; Wu, B.; Jiang, A.; You, G. A New-Type Ultraviolet SHG Crystal β-BaB_2O_4. *Sci. Sin. (Ser. B)* **1985**, *28*, 235−243.
(28) Chen, C.; Wu, Y.; Jiang, A.; Wu, B.; You, G.; Li, R.; Lin, S. New Nonlinear Optical Crystal LiB_3O_5. *J. Opt. Soc. Am. B* **1989**, *6*, 616−621.
(29) Mori, Y.; Kuroda, I.; Nakajima, S.; Sasaki, T.; Nakai, S. Nonlinear Optical Properties of Cesium Lithium Borate. *Jpn. J. Appl. Phys.* **1995**, *34*, L296−L298.
(30) Chen, C. T.; Wang, G. L.; Wang, X. Y.; Xu, Z. Y. Deep-UV Nonlinear Optical Crystal $KBe_2BO_3F_2$-Discovery, Growth, Optical Properties and Applications. *Appl. Phys. B Lasers Opt.* **2009**, *97*, 9−25.
(31) Straif, K.; Benbrahim-Tallaa, L.; Baan, R.; Grosse, Y.; Secretan, B.; El Ghissassi, F.; Bouvard, V.; Guha, N.; Freeman, C.; Galichet, L.; Cogliano, V. A Review of Human Carcinogens—Part C: Metals, Arsenic, Dusts, and Fibres. *Lancet Oncol.* **2009**, *10*, 453−454.
(32) Li, Z.; Lin, Z.; Wu, Y.; Fu, P.; Wang, Z.; Chen, C. Crystal Growth, Optical Properties Measurement, and Theoretical Calculation of BPO_4. *Chem. Mater.* **2004**, *16*, 2906−2908.
(33) Li, Z.; Wu, Y.; Fu, P.; Pan, S.; Chen, C. Flux Growth of BPO_4 Crystals. *J. Cryst. Growth* **2004**, *270*, 486−490.
(34) Yu, H.; Zhang, W.; Young, J.; Rondinelli, J. M.; Halasyamani, P. S. Design and Synthesis of the Beryllium-Free Deep-Ultraviolet Nonlinear Optical Material $Ba_3(ZnB_5O_{10})PO_4$. *Adv. Mater.* **2015**, *27*, 7380−7385.
(35) Yu, H.; Cantwell, J.; Wu, H.; Zhang, W.; Poeppelmeier, K. R.; Halasyamani, P. S. Top-Seeded Solution Crystal Growth, Morphology, Optical and Thermal Properties of $Ba_3(ZnB_5O_{10})PO_4$. *Cryst. Growth Des.* **2016**, *16*, 3976−3982.
(36) Hou, Y.; Zhang, B.; Wu, H.; Yu, H.; Hu, Z.; Wang, J.; Wu, Y. $K_3B_4PO_{10}$ and $K_2MB_4PO_{10}$ (M = Rb/Cs): Rare Mixed-Coordinated Borophosphates with Large Birefringence. *Inorg. Chem. Front.* **2021**, *8*, 1468−1475.
(37) Yu, S.; Wu, H.; Yu, H.; Hu, Z.; Wang, J.; Wu, Y. $NH_4(B_6PO_{10}(OH)_4){\cdot}H_2O$: Exhibiting the Largest Birefringence in Borophosphates. *Chem. Commun.* **2022**, *58*, 2834−2837.
(38) Zhang, W.; Huang, J.; Han, S.; Yang, Z.; Pan, S. Enhancement of Birefringence in Borophosphate Pushing Phase-Matching into the Short-Wavelength Region. *J. Am. Chem. Soc.* **2022**, *144*, 9083−9090.
(39) Wu, C.; Li, L.; Yang, G.; Song, J.; Yan, B.; Humphrey, M. G.; Zhang, L.; Shao, J.; Zhang, C. Low-Temperature-Flux Syntheses of Ultraviolet-Transparent Borophosphates $Na_4MB_2P_3O_{13}$ (M = Rb, Cs) Exhibiting a Second-Harmonic Generation Response. *Dalton Trans.* **2017**, *46*, 12605−12611.
(40) Wu, C.; Jiang, X.; Lin, L.; Dan, W.; Lin, Z.; Huang, Z.; Humphrey, M. G.; Zhang, C. Strong SHG Responses in a Beryllium-Free Deep-UV-Transparent Hydroxyborate via Covalent Bond Modification. *Angew. Chem., Int. Ed.* **2021**, *60*, 27151−27157.
(41) Bekker, T. B.; Podborodnikov, I. V.; Sagatov, N. E.; Shatskiy, A.; Rashchenko, S.; Sagatova, D. N.; Davydov, A.; Litasov, K. D. γ-BaB_2O_4: High-Pressure High-Temperature Polymorph of Barium

https://doi.org/10.1021/acsmaterialslett.2c00929
ACS Materials Lett. 2023, 5, 155−161

Borate with Edge-Sharing BO_4 Tetrahedra. *Inorg. Chem.* **2022**, *61*, 2340−2350.
(42) Lu, J.; Yue, J. N.; Xiong, L.; Zhang, W. K.; Chen, L.; Wu, L. M. Uniform Alignment of Non-π-Conjugated Species Enhances Deep Ultraviolet Optical Nonlinearity. *J. Am. Chem. Soc.* **2019**, *141*, 8093−8097.
(43) Brese, N. E.; O'Keeffe, M. Bond-Valence Parameters for Solids. *Acta Crystallogr. Sect. B Struct. Sci.* **1991**, *47*, 192−197.
(44) Sørensen, B. E. A Revised Michel-Lévy Interference Colour Chart Based on First-Principles Calculations. *Eur. J. Mineral.* **2013**, *25*, 5−10.
(45) Wu, Y.; Sasaki, T.; Nakai, S.; Yokotani, A.; Tang, H.; Chen, C. CsB_3O_5: A New Nonlinear Optical Crystal. *Appl. Phys. Lett.* **1993**, *62*, 2614−2615.
(46) Kurtz, S. K.; Perry, T. T. A Powder Technique for the Evaluation of Nonlinear Optical Materials. *J. Appl. Phys.* **1968**, *39*, 3798−3813.
(47) Kohn, W.; Sham, L. J. Self-Consistent Equations Including Exchange and Correlation Effects. *Phys. Rev.* **1965**, *140*, A1133−A1138.
(48) Krukau, A. V.; Vydrov, O. A.; Izmaylov, A. F.; Scuseria, G. E. Influence of the Exchange Screening Parameter on the Performance of Screened Hybrid Functionals. *J. Chem. Phys.* **2006**, *125*, 224106.
(49) Von Barth, U.; Hedin, L. A Local Exchange-Correlation Potential for the Spin Polarized Case. I. *J. Phys. C Solid State Phys.* **1972**, *5*, 1629−1642.
(50) Hasegawa, T.; Yamane, H. The Crystal Structure of $Li_2B_3PO_8$ with the 2D-Linkage of BO_3, BO_4 and PO_4 Groups. *Dalton Trans.* **2014**, *43*, 14525−14528.
(51) Li, Z.; Jin, W.; Zhang, F.; Chen, Z.; Yang, Z.; Pan, S. Achieving Short-Wavelength Phase-Matching Second Harmonic Generation in Boron-Rich Borosulfate with Planar [BO_3] Units. *Angew. Chem., Int. Ed.* **2022**, *61*, e202112844.

https://doi.org/10.1021/acsmaterialslett.2c00929
ACS Materials Lett. 2023, 5, 155−161